www.DeepakPublishing.com

Matandirotya E., et al. (2013): JoSS, Vol. 2, No. 1, pp. 133-146
(Peer-reviewed Article available at www.jossonline.com)

www.JoSSonline.com

Evaluation of a Commercial-Off-the-Shelf Fluxgate Magnetometer for CubeSat Space Magnetometry

Electdom Matandirotya[1], Robert R. Van Zyl[1], Daniel J. Gouws[2], and Elda F. Saunderson[2]

[1] *Cape Peninsula University of Technology, Faculty of Engineering, Department of Electrical Engineering, Bellville, Western Cape, South Africa*
[2] *South African National Space Agency: Space Science, Hermanus, Western Cape, South Africa*

Abstract

A low-cost, commercial-off-the-shelf (COTS) fluxgate magnetometer suitable for space magnetometry applications on a CubeSat mission is proposed as a cost effective science grade magnetometer. Three commercial-off-the-shelf fluxgate magnetometers were identified and evaluated against the following criteria: power efficiency, weight, noise, linearity and adaptability. The evaluation was concluded with environmental testing of the selected magnetometer, which included thermal cycling, functional temperature and vibration tests as a measure of space qualification of the instrument. Separation of the sensor and electronics was one of the major modifications to enable the sensor to be deployed on a boom, which is important to minimize magnetic interference from the satellite, while the electronics board is placed within the satellite body. The LEMI-011B fluxgate magnetometer passed the environmental tests and was proposed as suitable for CubeSat deployment. The performance characteristics of the magnetometer after modification and environmental tests are as follows: 0.7 nT (rms) noise at 12.83 Hz, ±2 nT over ±60000 nT non-linearity and 0.03 W power consumption.

1. Introduction

CubeSat developments at Universities offer a platform for students to realize space-based research goals within a short time frame and at relatively low cost. A CubeSat is a nano-satellite with standard dimensions of 100 x 100 x 100 mm and mass less than 1.33 kg. With this form factor the CubeSat is generally referred to as a “1U” (Munakata, 2009). The use of commercial-off-the-shelf (COTS) components in CubeSat designs

Corresponding Author: Electdom Matandirotya (Siziba), electdom@gmail.com
Publication History: Submitted – 03/13/13; Revision Accepted – 05/09/13; Published – 08/07/13

lowers its cost and development time. Considering the mass and volume of a CubeSat, associated payloads must be compatible with the satellite bus to avoid strain, especially on the satellite power budget, which is typically limited to 2- 3 W for a 1U. A candidate magnetometer is proposed for CubeSat space magnetometry. The work presented in this paper was conducted in parallel with the development of two CubeSats, a 1U and a 3U, by the students at the Cape Peninsula University of Technology under the F'SAT[1] nano-satellite development program.

The use of magnetometers in space dates back to 1958, when a fluxgate magnetometer was used for determining satellite orientation on Sputnik-3 (Diaz-Michelena, 2009). Magnetometers in satellite applications are used for either orientation purposes or as science-grade payloads. Orientation magnetometers are incorporated in the attitude determination and control system (ADCS) for the stabilisation of the satellite in orbit. Science-grade magnetometers are designed for defined scientific experiments such as measurements of the geomagnetic field in the vicinity of the satellite (Acuna, 2002). Magnetic measurements are a significant tool in the derivation of fundamental characteristics and behaviour of high energy particles and plasma in space, as well as mapping of the Earth's magnetic field (Langel et al., 1982; Olsen et al., 2003). During adverse space weather, i.e., during magnetic storms, the high energy particles have an influence on the Earth's magnetic field pattern and, hence, magnetic measurements aid in the understanding of the effects of such space weather events. (Space weather is defined as "conditions on the Sun and in the solar wind, magnetosphere, ionosphere, and thermosphere that can influence the performance and the reliability of space-borne and ground based technological systems, and can endanger human life" (Moldwin, 2008).)

Both vector (e.g., fluxgate; vector helium) and scalar (e.g., proton precession; optically pumped) magnetometers can be used for magnetic measurements in space (*see also* Acuna, 2002 and references therein), depending on the mission specification. Progressive technological advancement led to a shift from analogue to digital signal processing, which comes with the benefit of lower power consumption and reduction in overall size of the magnetometer unit (Ciudad et al., 2010; Forslund et al., 2007). A suitable deployment boom and a space-hardened enclosure are necessary to minimize magnetic interference from the main satellite body, as well as shield the sensor from radiation (Diaz-Michelena, 2009; O'Brien et al., 2007) respectively. The desired operational characteristics of a space-grade nano-satellite magnetometer are mechanical and thermal robustness, compact form factor, low power consumption, and low mass. Low noise levels and stable offsets enhance measurement accuracy. The measurement range of the magnetometers should be wide enough (above ±50000 nT) to accommodate the Earth's field, as well as any fluctuations resulting from space weather anomalies (Ciudad, 2010). The recommended attributes of a space magnetometer are listed in Table 1 (Balogh, 1999).

Table 1. Characteristics of Space Magnetometers (adopted from Balogh, 1999)

Measurement Range, nT	±60000
Band width, Hz	0 - 30
Resolution, nT	1 - 5
Noise, nT	< 5

The evaluation procedure, environmental tests and results are described. In this paper, we discuss the reasons which lead to the selection of the LEMI-011B fluxgate magnetometer as a candidate for use in space magnetometry for small satellites, and the necessary modifications required to the instrument.

2. Description and Selection of Fluxgate Magnetometer

Fluxgate magnetometers, which are vector magnetometers capable of measuring the strength and the direction of the magnetic field, generate an electrical

[1] French South African Institute of Technology (http://active.cput.ac.za/fsati/)

signal with a magnitude that is proportional to the intensity of the external magnetic field. The ferromagnetic cores of the sensor are periodically driven into saturation by an excitation current. In the presence of an external field, a voltage proportional to the field is induced on the pick-up coils. This voltage is then processed to give the magnitude of the external field. Fluxgates are used in the measurement of static (dc) or low frequency (ac) magnetic fields (Ripka, 2000; Ripka, 2003). Furthermore, fluxgate sensors have proved to combine good sensitivity, high stability and linearity, which can be realized at low power consumption levels (Acuna, 2002; Diaz-Michelena, 2009). A detailed principle of operation of the fluxgate magnetometers is given by Ripka (2003).

The fluxgate magnetometer type was chosen for its good trade-off between stability and volume, as well as its affordability. After a general market survey, based on the specifications documented by suppliers, the number of magnetometers evaluated was limited by the availability of the instruments, i.e., supplier delivery within the specified research period. Three fluxgate magnetometers were evaluated. All the magnetometers are COTS instruments that are designed primarily for industrial applications. LEMI-011T and LEMI-011B are products of the Lviv Institute of Space Research (Lviv Center of Institute of Space Research, 2009) and MF-1D is a product of Innalabs (Digital Magnetometer MF-1D, 2009). The magnetometers are shown in Figure 1. Table 2 shows the power and mass parameters of the selected candidate magnetometers. From the table it can be seen that the magnetometers identified are comparable in terms of these parameters.

3. Calibration, Evaluation and Modification

A tri-axial square Helmholtz coil system was used for the calibration of the magnetometer. The Helmholtz coil system is located in a dedicated, magnetically clean building within the premises of the South African National Space Agency (SANSA), Space Science Directorate (34.4 °S, 19.2 °E). The coil system has a custom designed control system with compensation algorithms for the dynamic cancellation of the Earth's magnetic field. Although the resolution of the dynamic compensation algorithms are 0.1 nT, the complete coils system has a worst case resolution of 3.5 nT.

3.1 Calibration Tests

Three significant tests were conducted during the calibration and evaluation process of the magnetom-

a)

b)

Figure 1. Pictures showing: a) the dimensions of MF_1D (adapted from the user's manual) and b) the LEM-011 fluxgate magnetometers. LEMI-011B is the box (black) version and LEMI-011T is the tube (white) version.

Table 2. Parameters of the three evaluated magnetometers.

Magnetometer	Mass (g) (Sensor + electronics)	Power supply (V)	Range (nT)	Power (W)	Sensitivity	Dimensions (mm)	Noise (ptp) (nT)
LEMI-011B	≤120	5 ± 0.25	± 60 000	0.03	27.4 (nT/mV)	55 x 51	2
LEMI-011T	≤120	5 ± 0.25	± 50 000	0.03	27.4 (nT/mV)	155 x 20	2
MF1D	155	9	± 70 000	1.5	(digital output)	55 x 44	2

eter, namely the so-called linearity, thin shell, and noise tests. The Earth's magnetic field was recorded during these tests to monitor any geomagnetic changes that may be detected during the test, and dynamic corrections were applied to the coils. The control algorithms of the different tests will not be discussed in this paper.

Linearity Test: A linearly varying magnetic field is generated in the coils system axes in 1000 nT step sizes at five seconds intervals from 60000 nT to 60000 nT. The result of this test is the difference between the data set of the applied magnetic field and the field measured by the magnetometer. The non-linearity (NL) of the magnetometer was calculated as the maximum difference between the applied and measured magnetic field data sets.

Thin Shell Test: The thin shell test is executed on a sensor placed in the Helmholtz coils to evaluate the sensor's response to the applied magnetic field. While the magnetometer is in the Helmholtz coil, a specific number of magnetic field vectors are applied, depending on the capabilities of the coils system and the desired level of accuracy. The vectors all have a constant magnitude, but random orientations, so as to create a three dimensional sphere of vectors. A spherical harmonic analysis algorithm is applied that "gives the spectral representation of the response of each magnetometer axis at a given field magnetic strength" (Risbo et al., 2000). The resultant matrix solution obtained from the algorithm contains information relating to the calibration parameters, such as the sensitivity, offsets, non-orthogonality and misalignments of each channel of the sensor. These parameters are applied in the calibration matrix for error compensation. For the particular test performed on the magnetometers in this paper, 200 vectors of 50000 nT magnitude were applied in the Helmholtz coils system. A detailed description of the Thin Shell Theorem and how the spherical harmonic model is applied during magnetometer calibration is described by Risbo et al. (2000) and also by Sipos et al. (2011).

Noise Test: The magnetometer is placed in a magnetically clean building with low magnetic noise or interference. No external magnetic field is applied to the magnetometer, and the output of the magnetometer is recorded at a frequency of 12.83 Hz (this frequency is not a documented specification, but what the test facilities are capable of executing). The standard deviation and the peak-to-peak noise of the recorded data are calculated. The Earth's magnetic field is recorded as a reference for any changes in the background magnetic field during the test.

3.2 Correction Matrix

The correction matrix consists of:

- Sensor sensitivity coefficients, which convert the measured output voltage of each magnetometer axes to a magnetic field strength in nT. They form the diagonal elements of the correction matrix.
- Sensor non-orthogonalities and misalignments form the off-diagonal elements of the correction matrix and correct for non-orthogonalities between the sensor axes and misalignment with the reference axes.

The calibration parameters are applied as indicated in Equation (1):

$$\begin{bmatrix} FieldX \\ FieldY \\ FieldZ \end{bmatrix} = \begin{bmatrix} C_{xx} & C_{xy} & C_{xz} \\ C_{yx} & C_{yy} & C_{yz} \\ C_{zx} & C_{zy} & C_{zz} \end{bmatrix} \times \begin{bmatrix} OutputX \\ OutputY \\ OutputZ \end{bmatrix} - \begin{bmatrix} OffsetX \\ OffsetY \\ OffsetZ \end{bmatrix} \tag{1}$$

Where:

Field(X,Y,Z) = measured fields for the three magnetometer axes in nT;
C_{xx}, C_{yy}, C_{zz} = sensor sensitivity for the x, y, z axes, respectively, in nT/mV;
C_{xy}, C_{xz}, C_{yx}, C_{yz}, C_{zx}, C_{zy} = non-orthogonalities and misalignments, in nT/mV;
Output(X,Y,Z) = voltage readings for each axis in mV;
Offsets(X,Y,Z) = the electronic offsets for each axis in nT.

3.3 Sensor Alignment

During the calibration of the magnetometer in the Helmholtz coils system, an alignment method known as current flipping was used. During current flipping, the field in the y-axis of the coils is flipped to a set positive and negative value. While flipping, no field is applied along the x-axis of the coils. The x-axis of the magnetometer is gradually rotated up to a point where the output of the x-axis of the magnetometer is the same for positive and negative y-fields. This implies that the x-axis of the magnetometer is measuring no field generated by the y-coils, but only representing the electronic offsets of the magnetometer; thus the x-axis of the magnetometer is orthogonal to the y-field of the coils. When orthogonality of the two axes has been achieved, the magnetometer is deemed to be aligned with the corresponding axis of the coils.

3.4 Calibration Results

The main criteria for the selection of the magnetometers were based on the sensor linearity and noise levels. The noise and linearity characteristics of the candidate magnetometers are shown in Figures 2 to 4, on the following page. The results explained in this section are calibration results derived before any modification of the magnetometers.

From Figure 2, though the linearity of the magnetometer was not well defined, the major concern was in the y axis, which seemed to have a cyclic variation when a positive field was applied. The problem was suspected to be due to a system error in the hardware, as more than one magnetometer of the same group had similar calibration results. The noise also exhibited a sinusoidal wave pattern with amplitudes of ~10 nT.

As illustrated in Figures 3 and 4, the LEMI 011B and LEMI 011T showed some similarity in the linearity pattern. A maximum of ± 3 nT non-linearity over ±60000 was recorded for the two magnetometers. The peak-to-peak noise of the LEMI-011B was lower than that of the LEMI 011T magnetometer. The similarities were expected, as the sensor configuration is similar and the only difference is in the electronics control boards. Table 3 is a further extraction of the results from the calibration tests. A result worth noting is the high, but stable, offsets of the LEMI 011B magnetometer after its first calibration tests. It was expected that these offsets would decrease significantly after the separation of the sensor and the electronics.

4. Modification

4.1 Rationale

A decisive step in the evaluation of the three magnetometers was the separation of the sensor from the electronics. The separation was necessary to reduce the magnetic interference from the current flowing within the enclosure. Modification warrants re-evaluation of their performance. Challenges in the modification of the magnetometers influenced the selection of the candidate magnetometer, as explained below.

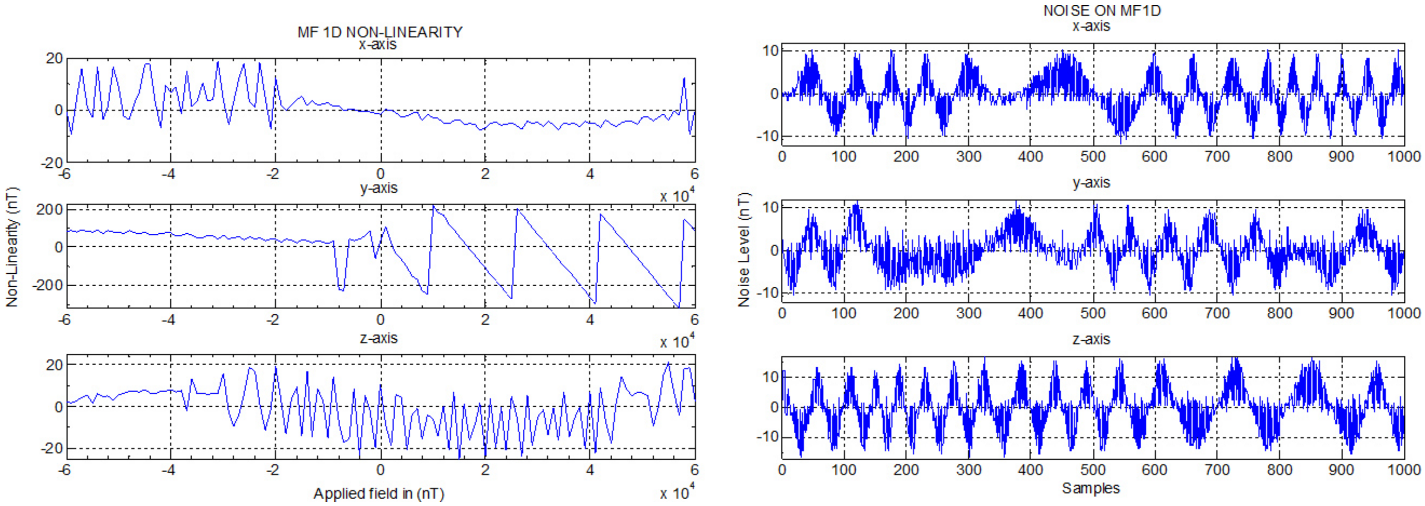

Figure 2. Graphical representation of the non-linearity and noise of the MF-1D magnetometer.

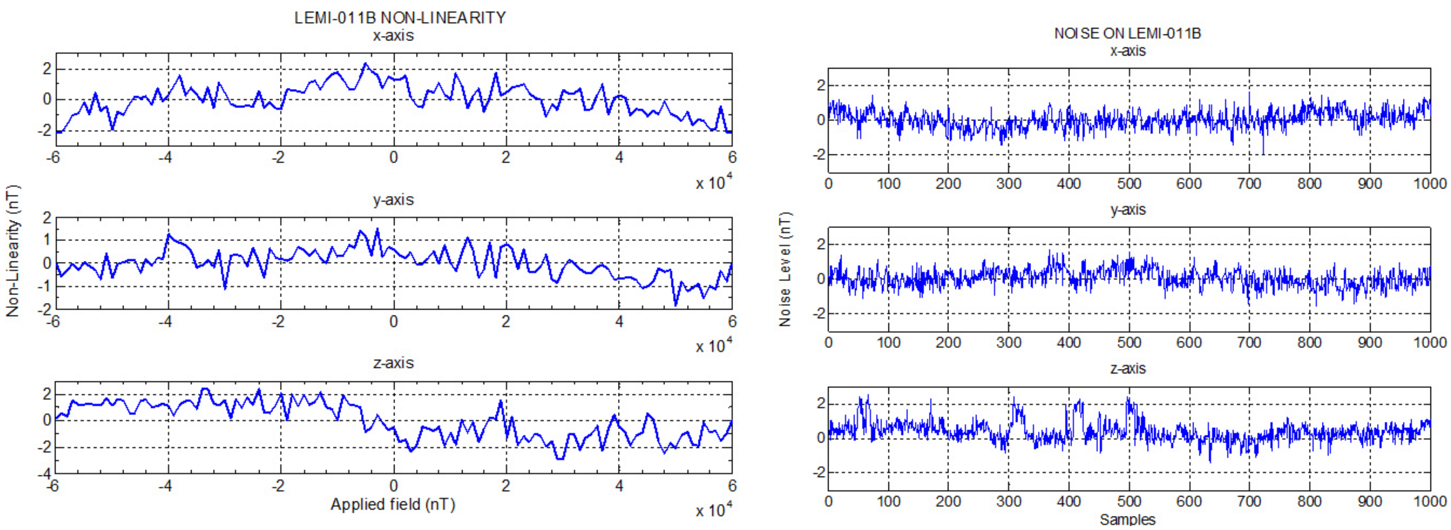

Figure 3. Graphical representation of the non-linearity and noise of the LEMI-011B magnetometer.

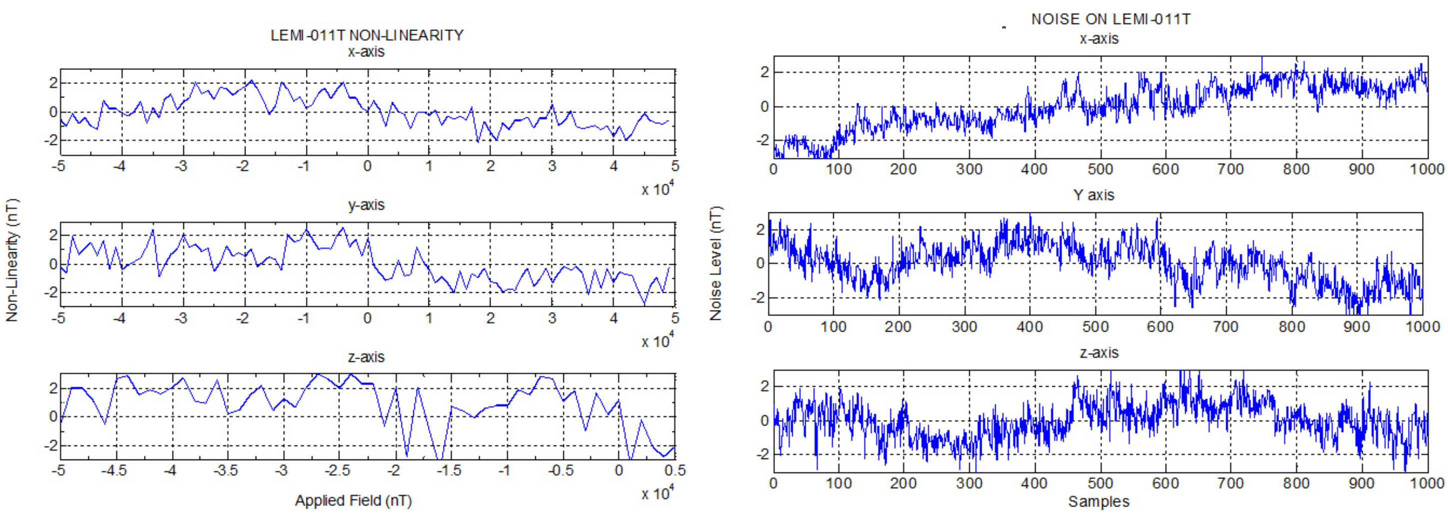

Figure 4. Graphical representation of the non-linearity and noise of the LEMI-011T magnetometer.

4.2 Modification Outcome

The sensor and electronics of the MF1D magnetometer could not be separated due to potting of the device, which limited further evaluation of the magnetometer. It was possible to separate the sensor of the LEMI 011T. However, the length of the electronics board (130 mm) would present integration challenges with the CubeSat form factor, so further evaluation of the magnetometer was not performed.

The 20 g (50 x 16 x 16 mm) LEMI 011B sensor was separated from the electronics. The LEMI 011B electronics board was found to be of a convenient size (51 mm × 55 mm), that could be fitted in either a 1U or 3U CubeSat without further structural modification. A 100 mm boom and enclosure (both made from aluminum) were designed for evaluation purposes. The designs are shown in Figure 5. A 9-pin connector and additional connecting wires were used to interface the sensor and its electronics through the hollow aluminum boom. Figure 6 illustrates the position of the sensor before and after separation.

Table 3. Calibration Performance of Selected Magnetometer.

	Axis	Noise (ptp) (nT)	Standard deviation of noise (nT)	Non-linearity (nT)	Output offsets (nT)	Separation of sensor and electronics
MF1D	x	22	4.631	18.5	252	Not possible
	y	22	4.636	300	-397	
	z	34	7.617	20	-457	
LEMI-011B	x	4	0.542	3	-1627	possible
	y	4	0.484	2	-1246	
	z	4	0.631	2	-1445	
LEMI-011T	x	6	1.302	3	-114	possible
	y	6	1.145	3	-67	
	z	7	1.077	3.5	57	

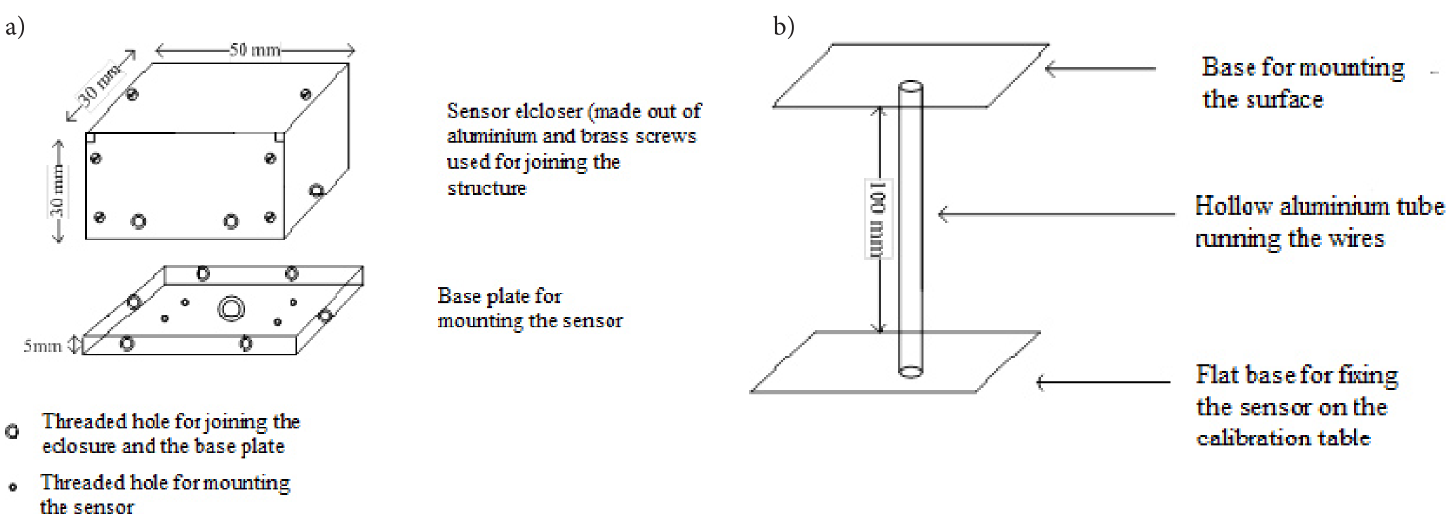

Figure 5. a) Preliminary enclosure and b) boom designed for calibration purposes.

Figure 6. The sensor position before and after separation.

5. Environmental Testing

An essential point to note when executing environmental tests is the element of misrepresentation of the space environment by the use of test chambers. The spacecraft (in this case the CubeSat) may have an orbital period of 100 min, and yet the chamber may not have the capacity to achieve the rapid temperature ramps desired. Thermal regions, which prescribe the temperature limits for qualification and acceptance testing, are determined by a dedicated thermal analysis team. Four proto-flight qualification level tests, i.e., the thermal vacuum, thermal cycling, functional temperature and vibration tests, were proposed to determine the robustness of the instrument to survive the launch and the harsh orbital environment (Korepanov, 2003). The thermal vacuum test could not be executed satisfactorily, because of technical problems experienced with the thermal vacuum test during the research period. These results are, therefore, not reported here. However, it is worth noting that the magnetometer did not fail during the test. Two environmental temperature tests were fully executed; the procedures are described in Appendix A.

5.1 Thermal Testing Margins

Three temperature margins are considered during the thermal testing of space-based instruments. These margins are cited by Gilmore (2002) and Goodman, et al. (2006) as:

Thermal Uncertainty Margin (TUM): This margin is considered a safety margin. The thermal uncertainty margin is applied as an additional temperature margin to the worst case predicted temperature limits.

Acceptance Test Thermal Margin (ATTM): This margin determines the maximum allowable temperature range for flight. It is added to both ends of the predicted worst case hot/cold temperature range. This margin is typically ± 5 °C.

Qualification Test Margin (QTM): This is the temperature above the expected operational environment temperature. It is a measure of the ruggedness of the device under test (DUT) design. Design flaws are exposed during the test.

In the presented results, the temperature values used during the test were as predicted by the satellite thermal models, excluding any TUM. These margins were applied according to the MIL-STD-1540B standards (EverySpec, 2009). The temperature ranges predicted (before applying the margins) for electronics within the satellite were + 5 °C to + 35 °C, while 10 °C to + 35 °C were predicted for electronics outside the satellite body. The added margins for the tests were ± 10 °C (ATTM) and ± 16 °C (QTM). The maximum qualification test temperature ranges were expected to be 11 °C to 61 °C for electronics within the satellite, and 26 °C to + 61 °C for electronics outside the satellite body.

5.2 Vibration Test

The vibration test is usually launcher-standardised. The main objective of the vibration test is to subject the instrument to the vibration profile of the launch vehicle in order to assess the structural integrity of the subsystem to withstand the forces that are exerted on it during launch.

Figure 7 shows the assembly of the electronics board and the sensor separately on the vibration jig. For this particular test, the vibration test limits applied to the magnetometers are shown in Figure 8. The specifications are derived from consolidating a standard that satisfies all specifications of potential launch vehicles as identified by survey. The maximum vibration amplitude that was used was 10.26 g rms. The sine levels listed in Table 4 were recommended at a sweep rate of 2 Octaves/min. The launch vehicles that were considered in the consolidation were the Dnepr, Soyuz, Strela, Volna, Falcon and PSLV. Their vibrations specifications are not given in this paper, but can be obtained from the respective operators.

Table 4. Specification of the Sinusoidal Levels During the Random Vibration Test.

Direction	Frequency band (Hz)	Sinusoidal amplitude (g or mm)
Longitudinal	4 - 10	10 mm peak to peak
Longitudinal	10 - 100	3.75 g
Lateral	2 - 8	10 mm peak to peak
Lateral	8 - 100	2.5 g

5.3 Temperature Cycle Test

Workmanship, material and process flaws can be detected during the temperature cycle test (Korepanov, 2003). Figure 9 illustrates the temperature profile inside and outside the chamber during the four prescribed temperature cycles. Several temperature sensors were used for temperature monitoring to enhance the accuracy of the measurements. The magnetometer

a)

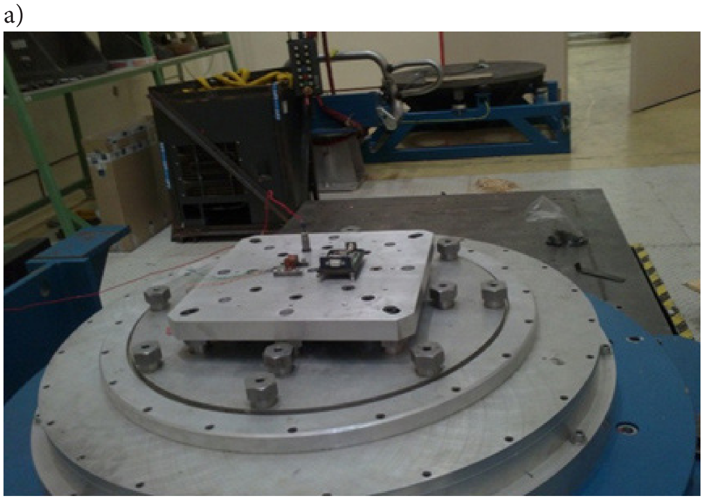

b)

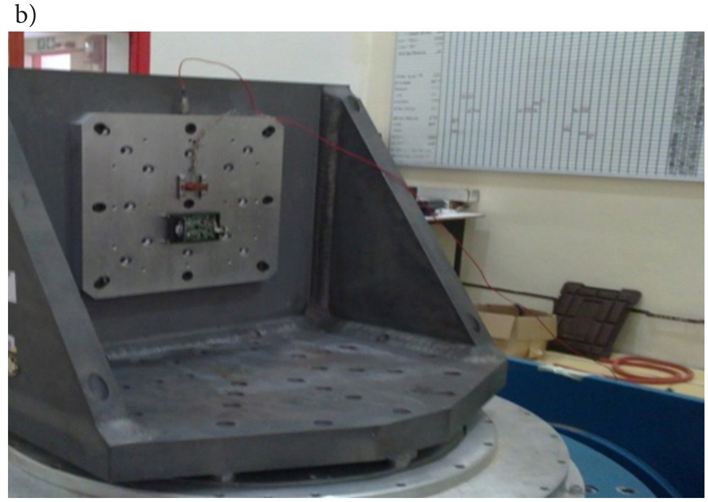

Figure 7. Mounting of the equipment on a vibration test jig a) set up for the transverse random test and b) for the longitudinal and vibration tests.

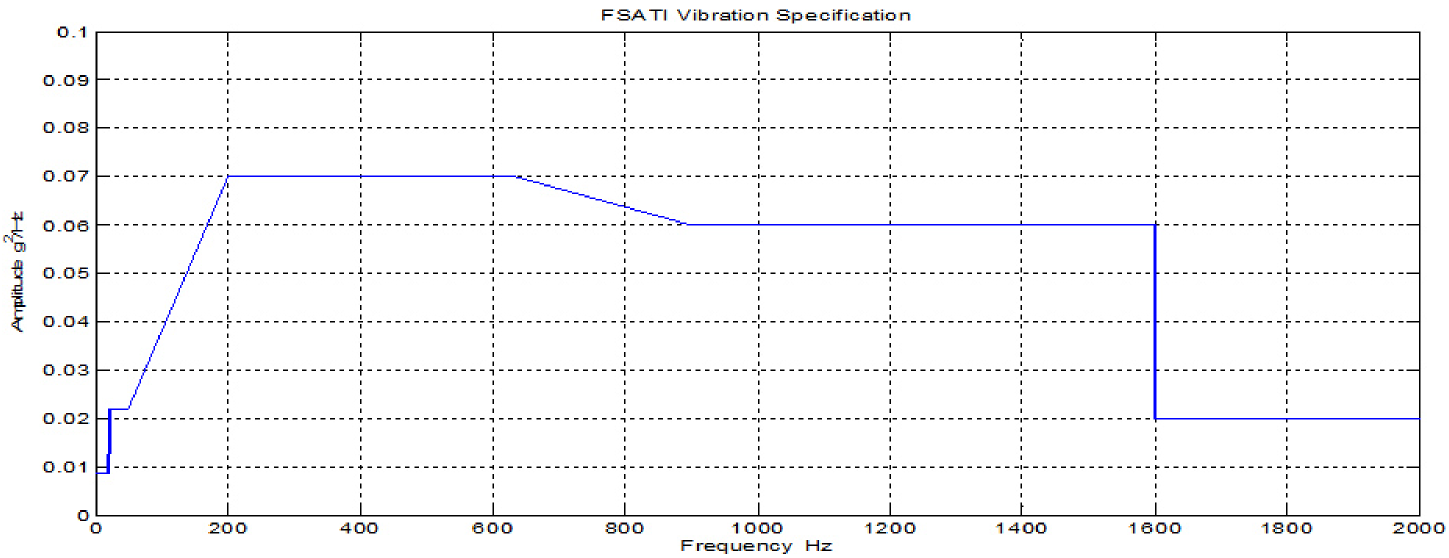

Figure 8. F'SATI vibration test limits.

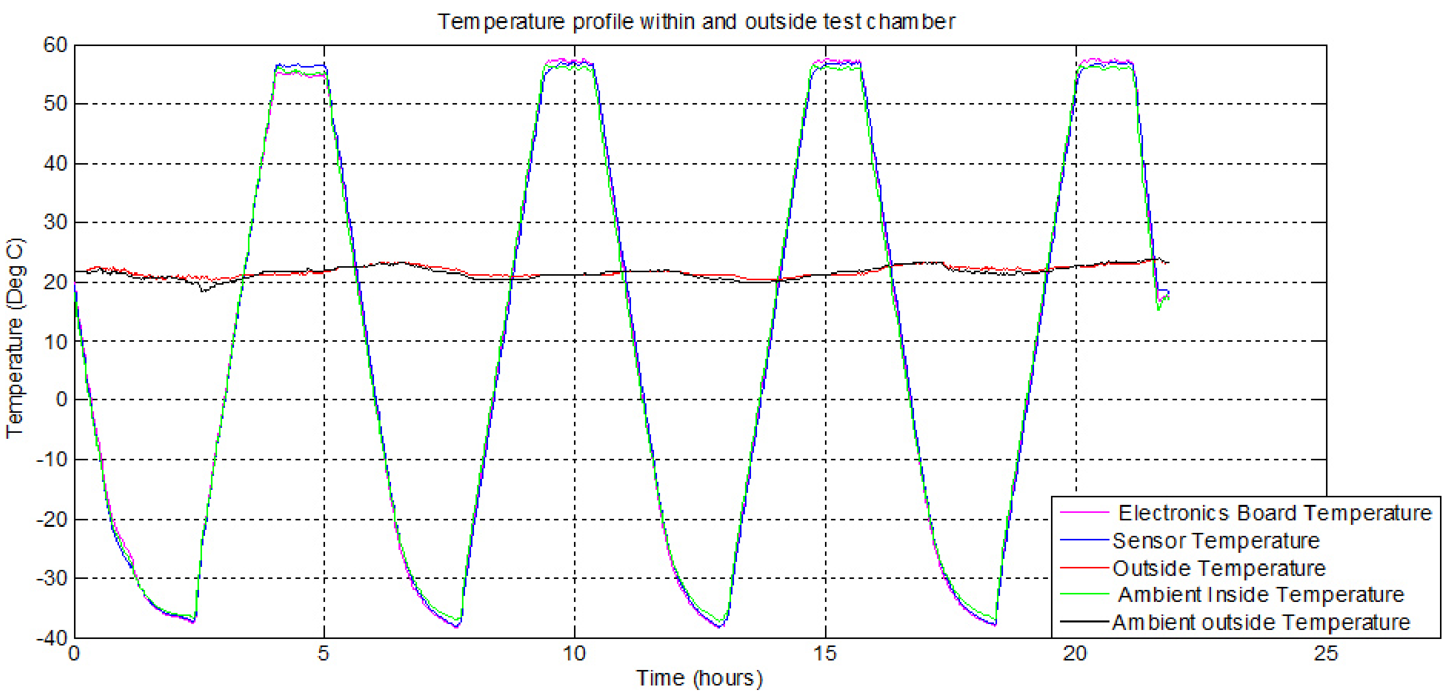

Figure 9. Temperature profile in the chamber during the temperature cycle test.

was switched off during the temperature cycle test. The procedure and temperature limits are reported in Table A1 of Appendix A.

5.4 Functional Temperature Test

The functional temperature test verifies the functionality of the instrument within the design temperature range as determined by the thermal model. The temperatures of the electronic board and the sensor were monitored. Figure 10 (next page) shows the temperature profile within the test chamber. The magnetometer was switched on and off at different intervals, including a hot start at maximum temperature (61 °C) and a cold start at the minimum temperature (26 °C), while verifying its functionality. The procedure and temperature limits are reported in Table A2 of Appendix A.

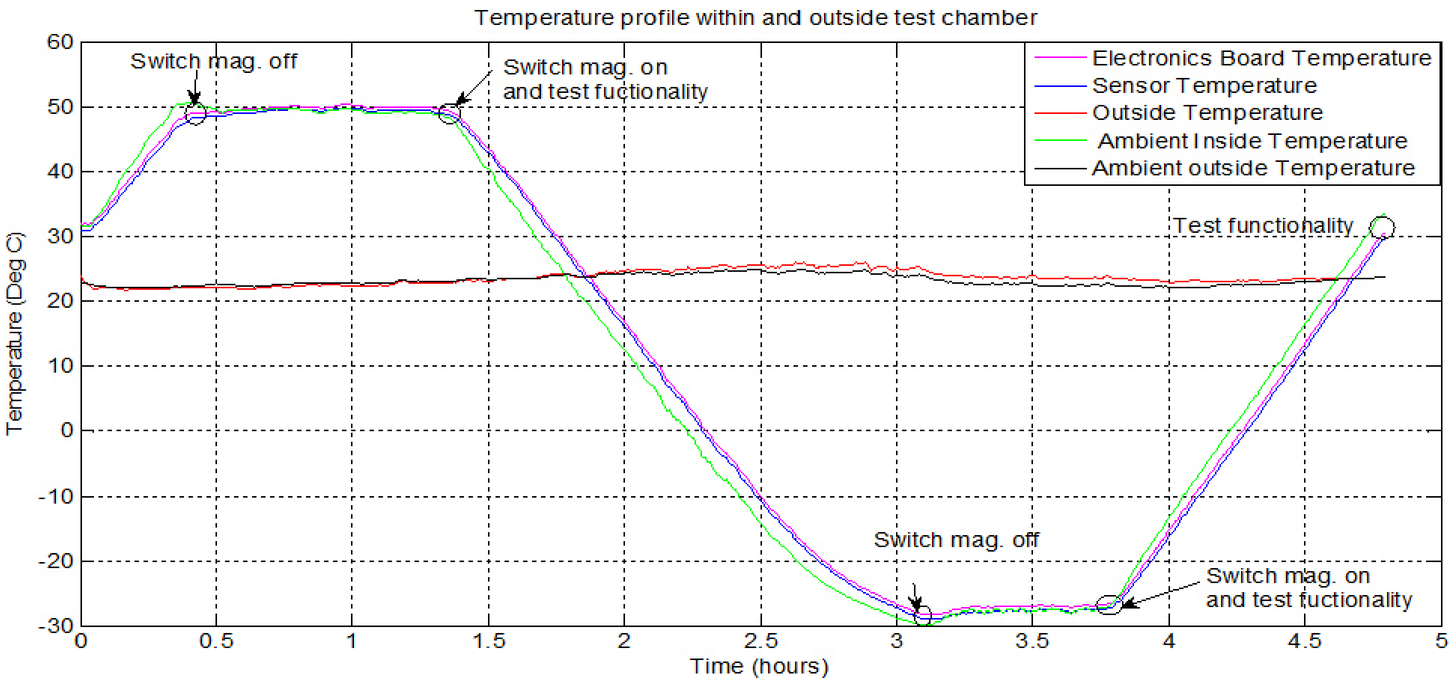

Figure 10. Temperature profile within the test chamber during the functional temperature test.

6. Performance Analysis

To evaluate the functionality of the magnetometer after every environmental test, a re-calibration process was performed on the modified magnetometer. The purpose of the re-calibration process was to evaluate the effects of the environmental tests on the performance of the magnetometer.

Tables 5 and 6 (next page) show the sensor parameters after each stage of environmental testing. The significant drop in the electronic offsets of the sensor after separation from the electronics is notable in Table 5. The reduction in the offsets can be ascribed to the increased distance between the sensor and the electronics, as the permanent magnetism of the electronics would affect the sensor. The sensitivity of the sensor was also affected slightly; however, it continued to be stable after sensor separation. Furthermore, it can be seen from Table 5 that there are relatively small differences in the offsets of the separated sensor after each environmental test. These differences may have resulted from misalignment of the sensor axes and the corresponding Helmholtz coil axes during the calibration process. These differences are not critical at this stage, as the final magnetometer offsets will be determined during *in situ* calibration of the magnetometer on the satellite before launch.

Table 6 shows the sensor noise and the standard deviation of the noise after each step of the modification, and environmental tests. The noise levels listed in Table 6 show that the modification and environmental tests did not degrade the performance of the magnetometer significantly; thus, harsh orbital conditions should not have a negative impact on the noise of magnetometer, which is a significant measure of magnetometer stability.

7. Recommendation and Conclusion

The LEMI-011B magnetometer is proposed for nano-satellite space magnetometry or for ADCS. The magnetometer, which is a tri-axial sensor, was selected as the best among the three magnetometers that were evaluated, based on the supporting performance parameters shown in Table 3. It exhibits good linearity over its measurement range, as indicated in Figure 3. The modified LEMI-011B sensor passed the environmental tests to which it was subjected. A space-qualified and space weather resistant enclosure can be designed so that the sensor is well protected. The LEMI-011B can be obtained from the suppliers at less than US$600 per unit. Additional modification, which may include development of a digital interface as the original magnetometer has an analogue interface, can be achieved in a standard laboratory.

Further research is required to assess if the separation of 100 mm between the sensor and the satellite frame is sufficient to mitigate the influence of the magnetic characteristics of a typical CubeSat bus.

Table 5. Sensor Sensitivity and Offset of the Modified LEMI-011B During the Different Stages of the Evaluation.

Evaluation stage	x-axis	y-axis	z-axis
Sensor sensitivity (mV/nT)			
Before separation	27.50	27.34	27.44
After separation of sensor and electronics	26.47	26.50	26.50
After vibration test	26.47	26.51	26.49
After temperature cycle test	26.46	26.51	26.48
After temperature functionality test	26.46	26.51	26.48
Sensor offset (nT)			
Before separation	1638	1233	1461
After separation of sensor and electronics	89.24	83.55	32.73
After vibration test	87.12	117.84	75.84
After temperature cycle test	106.7	99.20	60.11
After temperature functionality test	97.94	107.83	114.73

Table 6. Noise Characteristics of the Modified LEMI-011B Sensor During Different Stages of Evaluation.

Evaluation stage	x-axis	y-axis	z-axis	Average
Peak to peak (ptp) noise (nT)				
Before separation	3.995	3.421	4.194	3.870
After separation of sensor and electronics	4.743	3.878	3.878	4.166
After vibration test	4.743	3.160	3.591	3.831
After temperature cycle test	4.722	3.864	4.007	4.198
After temperature functionality test	5.154	3.578	3.434	4.055
Standard deviation of the noise (nT)				
Before separation	0.542	0.484	0.632	0.553
After separation of sensor and electronics	0.762	0.552	0.723	0.679
After vibration test	0.724	0.518	0.575	0.606
After temperature cycle test	0.723	0.631	0.746	0.700
After temperature functionality test	0.760	0.576	0.563	0.633

Appendix

TEMPERATURE CYCLE AND FUNCTIONAL TEMPERATURE TESTS: PROCEDURES AND TEMPERATURE LIMITS

Table A1. Temperature Cycle Test Procedure

Procedure	1. Perform the functional tests at ambient temperature 2. Cool down to low temperature (power off) 3. Allow 1 hour dwell time at the minimum extreme temperature 4. Increase temperature to maximum extreme 5. Allow 1 hour dwell time at maximum extreme temperature 6. Decrease temperature to ambient 7. Repeat steps 2 to 6 for four cycles for acceptance 8. Perform functional tests at ambient temperature after completion	
Pressure level:	Ambient	
Temperature Limits:	Inside spacecraft:	
	Qualification	Acceptance
	Maximum extreme +61 °C	Maximum extreme +51 °C
	Minimum extreme -21 °C	Minimum extreme -11 °C
	Outside spacecraft:	
	Maximum extreme +61 °C	Maximum extreme +51 °C
	Minimum extreme -36 °C	Minimum extreme -26 °C
Gradient: During heating:	During heating:1 °C/min (nominal)	
	During cooling:0.2 °C/min (nominal)	
Number of Cycles:	4 cycles (Qualification); 2 cycles (Acceptance)	

Table A2. Functional Temperature Test procedure

Procedure	1. Start at ambient temperature (power on) 2. Perform the functional tests 3. Increase temperature to the maximum extreme (with power on) 4. Switch off the power of the test item 5. Allow 1 hour dwell time at the maximum extreme temperature 6. Perform a hot start and repeat functional tests 7. Cool down to minimum extreme (with power on) 8. Switch off power of the test item 9. Allow 1 hour dwell time at the minimum extreme temperature 10. Perform a cold start and repeat functional tests 11. Allow test item to return to ambient temperature (with power on) 12. Repeat functional tests	
Pressure level:	Ambient	
Temperature Limits:	Inside Space Craft	Inside Space Craft
	Maximum extreme +51 °C	Maximum extreme +51 °C
	Minimum extreme -11 °C	Minimum extreme -26 °C
Gradient: During heating:	During heating: 1 °C/min (nominal)	
	During cooling: 0.2 °C/min (nominal)	
Number of Cycles:	One	

Acknowledgements

The opportunity to use the facilities of SANSA Space Science[2], ISSA[3], SunSpace[4] and the University of Stellenbosch[5] throughout the calibration and environmental testing is greatly appreciated.

References

Acuna, M. H. (2002): Space-based magnetometers. *Review of Scientific Instruments,* Vol.73, pp. 3717-3736.

Balogh, A. (1999): Space instrumentation. *Space and Atmospheric Physics.* Available: www.sp.ph.ic.ac.uk/~balogh/spinstr.htm. [Accessed 12 March 2011].

Ciudad, A., et al. (2010): Small fluxgate magnetometers: development and future trends in Spain, *Sensors*, Vol. 10, pp. 1859-1870.

Diaz-Michelena, M. (2009): Small magnetic sensors for space applications. *Sensors*, Vol. 9, pp. 2271-2288.

Digital Magnetometer MF-1D. (2009): Technical reference and user's manual. Available: http://www.innalabs.com/ [Accessed 14 November 2010].

EverySpec, (2009): Military standard: test requirements for space vehicles (10 Oct 1982). Available: www.everyspec.com/MIL-STD/MIL-STD-1540_17789/ [Accessed 25 March 2011].

Forslund, A., et al. (2007.): Miniaturized digital fluxgate magnetometer for small spacecraft applications. *Measurement Sci. and Tech.*, Vol. 19. pp 1-10.

Gilmore, D. G. (2002): *Spacecraft Thermal Control Handbook: Fundamental Technologies, Vol. 1*. El Segundo, California: The Aerospace Press.

Goodman, J., et al. (2006): Environmental (thermal) testing of space instrumentation: the GLAST example. *Nucl. Instruments & Methods in Physics Research A,* Vol. 563, pp. 377-380.

Korepanov, V. E., (2003): The modern trends in space electromagnetic instrumentation. *Advanced Space Research*, Vol. 32, pp. 401-406.

Langel, R., et al. (1982): The MAGSAT mission. *Geophysics Research Letter*, Vol. 9, pp. 243-245.

Lenz, J. and Edelstein, A. S. (2006): Magnetic sensors and their application. *Sensors*, Vol. 3, pp. 631-648.

LvivCenter of Institute of Space Research. (2009): Available: http://www.isr.lviv.ua/lemi011.htm [Accessed 3 June 2011].

Merayo, J M G, et al. (2000): Scalar calibration of vector magnetometers. *Measurement Sci. and. Tech. l.* Vol. 11, pp. 120–132.

Munakata, R. (2009): CubeSat design specifications. Available: www.cubesat.org/index.php/documents/develpers [Accessed 18 March 2013].

Moldwin, M. (2008): *An introduction to space weather.* New York: Cambridge University Press.

O'Brien H., et al. (2007): A radiation tolerant digital fluxgate magnetometer. *Measurement Sci. and Tech.*. Vol. 18, pp. 3645-3650.

Olsen, N., et al. (2003): Calibration of the Ørsted vector magnetometer. *Earth Planets Space*, Vol. 55, pp. 11-18.

Quintero, A.H., et al. (1999): Perceptiveness of thermal vacuum testing presented at the 18th Aerospace Testing Seminar, 16-18 March. Los Angeles, CA.

Ripka, P. (2000): Advances in flux-gate sensors. *Sensors and Actuators.* A. Vol. 106, pp. 8-14.

Risbo, T., et al. (2001): Ørsted calibration mission: the thin shell method and spherical harmonic analysis." *Ground and In-Flight Space Magnetometer Calibration Techniques*, ESA SP-490.

Sipos, M., et al. (2011): Improvement of electronic compass accuracy based on magnetometer and accelerometer calibration, in *Proc. 10th Symposium Magnetic Measurements*, Warsaw.

[2] South African National Space Agency: Space Science, Hermanus, South Africa http://www.sansa.org.za)

[3] Institute for Satellite and Software Application, Houwteq, Grabouw, South Africa

[4] SunSpace, Stellenbosch, South Africa

[5] University of Stellenbosch, Stellenbosch, South Africa